# Retrieving the thermal diffusivity and effusivity of solids from the same frequency scan using the front photopyroelectric technique

Agustín Salazar [1,*], Alberto Oleaga [1], Arantza Mendioroz [1] and Estibaliz Apiñaniz [2]

[1] Departamento de Física Aplicada I, Escuela de Ingeniería de Bilbao, Universidad del País Vasco UPV/EHU, Plaza Ingeniero Torres Quevedo 1, 48013 Bilbao, Spain.
[2] Departamento de Física Aplicada I, Escuela Universitaria de Ingeniería de Vitoria-Gasteiz, Universidad del País Vasco UPV/EHU, Nieves Cano 12, 01006 Vitoria-Gasteiz, Spain.
* Corresponding author.
E-mail Address: agustin.salazar@ehu.es

## Abstract

The photopyroelectric (PPE) technique in the front configuration consists in illuminating one surface of a pyroelectric slab while the other surface is in contact with the test sample. This method has been widely used to measure the thermal effusivity of liquids. Recently, it has been extended to measure the thermal effusivity of solids, by taking into account the influence of the coupling fluid layer used to guarantee the thermal contact. In both cases, the sample (liquid or solid) must be very thick. In this work, we propose a classical frequency scan of a thin sample slab to retrieve the thermal diffusivity and effusivity simultaneously. We use the amplitude and the phase of the front PPE signal, which depend on four parameters: the sample diffusivity and effusivity, the coupling fluid thickness and the coefficient of heat losses. It is demonstrated that the four quantities are not correlated. PPE measurements performed on a set of calibrated solids confirm the ability of the method for obtaining the thermal diffusivity and effusivity of solids accurately.

Keywords: thermal effusivity, thermal diffusivity, photopyroelectric technique, photothermal techniques

## 1. Introduction

Since the introduction of the photopyroelectric (PPE) technique by Mandelis and Zver in 1985 [1], it has been widely used to measure the thermal properties of solid and liquids due to its exceptional signal to noise ratio. In a PPE device the test sample is in thermal contact with a pyroelectric slab, which senses temperature variations. In the back configuration the free surface of the sample is illuminated by a modulated light beam, while in the front configuration the free surface of the pyroelectric sensor is illuminated. In both configurations the PPE current produced by the pyroelectric sensor depends on the thermal diffusivity ($D$) and effusivity ($e$) of the sample under study.

The PPE technique in the back configuration, with thermally thick sample and sensor, allows measuring $D$ and $e$ simultaneously from simple linear relations [2-3]. This method has been used to measure these thermal properties in liquids across phase transitions (see Ref. 4 and references therein). However, in the case of solid samples, a very thin grease layer must be used to assure the thermal contact between the sample and the detector. It has been demonstrated that even a few microns thick fluid layer produces an underestimation of $D$ and $e$, which is more pronounced for good thermal conductors [5]. To overcome this underestimation it has been proposed to use a transparent pyroelectric sensor and a transparent coupling fluid, together with a self-normalization procedure [6]. In this modified setup the amplitude and phase of the self-normalized PPE signal behaves linearly as a function of the square root of the modulation frequency, but unlike in the standard back configuration with an opaque sensor, the slope does not depend on the fluid layer. This means that the thermal diffusivity can be obtained accurately, but the price to be paid is loosing information on the thermal effusivity of the solid.

The PPE technique in the front configuration was introduced by Dadarlat and coworkers [7]. In the case of a very thick sample it provides an accurate method to measure the thermal effusivity of liquids [8]. The method consists in heating the free surface of the pyroelectric sensor and recording the PPE signal twice, first with the liquid wetting the back surface of the detector and then with the bare detector. The normalized PPE signal is obtained as the ratio of both signals, which is independent of the instrumental factor (the frequency dependence of the detection electronics), of the electrical properties of the sensor and of the laser intensity. It is demonstrated that the frequency scan of this normalized signal is highly sensitive to the thermal effusivity of the backing liquid [9,10]. This method cannot be applied straightforward to solid samples, since the coupling fluid layer modifies the normalized PPE signal, so the thermal effusivity cannot be obtained accurately.

To overcome this issue, in a previous work authors proposed a frequency scan of the PPE signal in the front configuration using a three-layer model: pyroelectric sensor, coupling fluid and very thick test solid [11]. As the thickness and thermal properties of the pyroelectric sensor, as well as the thermal properties of the fluid are known, it was demonstrated that the normalized PPE signal only depends on two unknown parameters: the solid effusivity and the thickness of the coupling fluid layer.

In this manuscript, we extend this previous work to measure the thermal effusivity and diffusivity of solids simultaneously using a frequency scan in the front configuration. The frequency range must be selected in such a way that the thickness of the solid slab changes from thermally thick to thermal thin along the frequency scan. We have developed a complete model including heat conduction in a five-layer model (air, pyroelectric sensor, coupling fluid, test solid and air) and heat losses by convection and radiation. Provided the thickness and thermal properties of the pyroelectric sensor, as well as the thermal properties of the fluid are known, we demonstrate that the normalized PPE signal depends on four unknown parameters: the solid effusivity and diffusivity, the thickness of the coupling fluid layer and

the coefficient of heat losses. Besides, from a sensitivity analysis, we show that the four parameters are uncorrelated and that the normalized PPE signal is highly sensitive to the thermal effusivity and diffusivity of the solid sample. PPE measurements performed on a set of calibrated solids confirm the ability of the method to obtain the thermal effusivity of solids accurately. Moreover, for each material, measurements on samples with varying thicknesses have been performed to verify the robustness of the method.

## 2. Theory

Let us consider a three-layer stack made of an opaque pyroelectric slab of thickness $L_p$, a fluid layer of thickness $L_f$ and a solid layer of thickness $L_s$. Both sides of this system are surrounded by air. The free surface of the pyroelectric slab is illuminated by a laser beam whose intensity $I_o$ is modulated at a frequency $f$ ($\omega = 2\pi f$). The geometry of the problem is shown in Fig. 1a. The PPE signal ($S$) is proportional to the spatially averaged temperature of the pyroelectric slab $\langle T_p \rangle$ [12],

$$S = ab\langle T_p \rangle = ab\frac{1}{L_p}\int_{-L_p}^{0} T_p(z)dz\,, \tag{1}$$

where $a$ is a frequency-independent factor that depends on the physical properties of the detector (pyroelectric coefficient, dielectric constant and permittivity) and $b$ is a frequency-dependent factor that accounts for the influence of the detection electronics.

The temperature of the pyroelectric slab is obtained by solving the heat diffusion equation for the five-layer system shown in Fig. 1a. The temperature at each layer is given by

$$T_{gf}(z) = Me^{-q_g z} \tag{2a}$$

$$T_p(z) = Ae^{q_p z} + Be^{-q_p z} \tag{2b}$$

$$T_f(z) = Ce^{q_f (z+L_p)} + Ee^{-q_f (z+L_p)} \tag{2c}$$

$$T_s(z) = Fe^{q_s (z+L_p+L_f)} + Ge^{-q_s (z+L_p+L_f)}\,, \tag{2d}$$

$$T_{gr}(z) = Ne^{q_g (z+L_p+L_f+L_s)} \tag{2e}$$

where $q = \sqrt{i\omega / D}$ is the thermal wave vector, being $D$ the thermal diffusivity. Subscripts $gf$ $p$, $f$ , $s$ and $gr$ stand for the gas at the front surface, the pyroelectric detector, the coupling fluid, the sample and the gas at the rear surface respectively. The eight constants in Eqs. (2) are obtained from the boundary conditions at the interfaces:

(a) Temperature continuity:

$$T_{gf}\Big|_{z=0} = T_p\Big|_{z=0} \qquad T_p\Big|_{z=-L_p} = T_f\Big|_{z=-L_p} \qquad T_f\Big|_{z=-(L_p+L_f)} = T_s\Big|_{z=-(L_p+L_f)}$$

$$T_s\Big|_{z=-(L_p+L_f+L_s)} = T_{gr}\Big|_{z=-(L_p+L_f+L_s)} \tag{3a}$$

(b) Heat flux continuity at the solid-fluid interfaces:

$$K_p\frac{dT_p}{dz}\Big|_{z=-L_p} = K_f\frac{dT_f}{dz}\Big|_{z=-L_p} \qquad K_f\frac{dT_f}{dz}\Big|_{z=-(L_p+L_f)} = K_s\frac{dT_s}{dz}\Big|_{z=-(L_p+L_f)} \tag{3b}$$

(c) Illumination and heat losses at the solid-air interfaces:

$$K_p\frac{dT_p}{dz}\Big|_{z=0} = K_g\frac{dT_g}{dz}\Big|_{z=0} + \frac{I_o}{2} - hT_{gf}\Big|_{z=0}$$

$$K_s\frac{dT_s}{dz}\Big|_{z=-(L_p+L_f+L_s)} = K_g\frac{dT_{gr}}{dz}\Big|_{z=-(L_p+L_f+L_s)} + hT_{gr}\Big|_{z=-(L_p+L_f+L_s)}\,. \tag{3c}$$

Here $K$ is the thermal conductivity and $h$ is the linear coefficient of heat transfer by convection and radiation, which is assumed to be the same at both surfaces since the temperature rise in PPE experiments is very small (< 1 K). Moreover, By substituting Eqs. (2) into Eqs. (3), the temperature of the pyroelectric slab is obtained. Then, from Eq. (1), the PPE signal ($S$) is calculated.

For normalization purposes, i.e. to eliminate the frequency dependence of the detection electronics, the PPE signal obtained for the five-layer system is divided by the PPE signal obtained for the bare pyroelectric slab surrounded by air. Its temperature can be obtained by solving the heat diffusion equation for the three-layer system shown in Fig. 1b

$$T_{gf}^{'}(z) = M' e^{-q_g z} \tag{4a}$$

$$T_{p}^{'}(z) = A' e^{q_p z} + B' e^{-q_p z} \tag{4b}$$

$$T_{gr}^{'}(z) = N' e^{q_g (z+L_p)}. \tag{4c}$$

Constants $M$', $A$', $B$' and $N$' are obtained from the boundary conditions at the interfaces:

(a) Temperature continuity:

$$T_{gf}^{'}\Big|_{z=0} = T_{p}^{'}\Big|_{z=0} \qquad T_{p}^{'}\Big|_{z=-L_p} = T_{gr}^{'}\Big|_{z=-L_p} \tag{5a}$$

(b) Illumination and heat losses at the surfaces:

$$K_p \frac{dT_p^{'}}{dz}\Big|_{z=0} = K_g \frac{dT_{gf}^{'}}{dz}\Big|_{z=0} + \frac{I_o}{2} - hT_{gf}^{'}\Big|_{z=0} \qquad K_p \frac{dT_p^{'}}{dz}\Big|_{z=-L_p} = K_g \frac{dT_{gr}^{'}}{dz}\Big|_{z=-L_p} + hT_{gr}^{'}\Big|_{z=-L_p}. \tag{5b}$$

As before, we have assumed that the coefficient $h$ is the same at both surfaces.

Once the pyroelectric sensor temperature is obtained, the normalized PPE signal ($S_n$) writes

$$S_n = \frac{S_{five-layer}}{S_{pyro}} = \frac{ab\langle T_p \rangle_{five-layer}}{ab\langle T_p \rangle_{pyro}} = \frac{A0\left[B0 + C0 + (1+e^{2q_f L_f})(D0 - E0)\right]}{A1 + B1 + 4(1+e^{2q_f L_f})e^{q_p L_p} e^{q_s L_s}(C1 + D1)}, \tag{6}$$

where

$$A0 = \left(-1 + e^{q_p L_p}\right)\left[\frac{e_p}{e_f} + \left(\frac{e_g}{e_f} + \frac{h}{e_f\sqrt{i\omega}}\right)\mathrm{cotgh}\left(\frac{q_p L_p}{2}\right)\right], \tag{7a}$$

$$B0 = \frac{e_p}{e_f}\frac{e_s}{e_f}\left(-1 + e^{2q_f L_f}\right)\left(1 + e^{q_p L_p}\right)\left[\frac{e_g}{e_f} + \frac{h}{e_f\sqrt{i\omega}} - \frac{e_s}{e_f} + e^{2q_s L_s}\left(\frac{e_g}{e_f} + \frac{h}{e_f\sqrt{i\omega}} + \frac{e_s}{e_f}\right)\right], \tag{7b}$$

$$C0 = \left(-1 + e^{2q_f L_f}\right)\left(-1 + e^{q_p L_p}\right)\left[-\frac{e_g}{e_f} - \frac{h}{e_f\sqrt{i\omega}} + \frac{e_s}{e_f} + e^{2q_s L_s}\left(\frac{e_g}{e_f} + \frac{h}{e_f\sqrt{i\omega}} + \frac{e_s}{e_f}\right)\right], \tag{7c}$$

$$D0 = e^{2q_s L_s}\left(\frac{e_g}{e_f} + \frac{h}{e_f\sqrt{i\omega}} + \frac{e_s}{e_f}\right)\left[\left(1 + e^{q_p L_p}\right)\frac{e_p}{e_f} + \left(-1 + e^{q_p L_p}\right)\frac{e_s}{e_f}\right], \tag{7d}$$

$$E0 = \left(\frac{e_g}{e_f} + \frac{h}{e_f\sqrt{i\omega}}\frac{e_s}{e_f}\right)\left[\frac{e_p}{e_f} + \frac{e_s}{e_f} + e^{q_p L_p}\left(\frac{e_p}{e_f} - \frac{e_s}{e_f}\right)\right], \tag{7e}$$

$$A1=\frac{e_p}{e_f}\frac{e_s}{e_f}\left(-1+e^{2q_fL_f}\right)\left[\frac{e_g}{e_f}+\frac{h}{e_f\sqrt{i\omega}}-\frac{e_p}{e_f}+e^{2q_pL_p}\left(\frac{e_g}{e_f}+\frac{h}{e_f\sqrt{i\omega}}+\frac{e_p}{e_f}\right)\right]\times \left[\frac{e_g}{e_f}+\frac{h}{e_f\sqrt{i\omega}}-\frac{e_s}{e_f}+e^{2q_sL_s}\left(\frac{e_g}{e_f}+\frac{h}{e_f\sqrt{i\omega}}+\frac{e_s}{e_f}\right)\right] \tag{7f}$$

$$B1=\left(-1+e^{2q_fL_f}\right)\left[-\frac{e_g}{e_f}-\frac{h}{e_f\sqrt{i\omega}}+\frac{e_p}{e_f}+e^{2q_pL_p}\left(\frac{e_g}{e_f}+\frac{h}{e_f\sqrt{i\omega}}+\frac{e_p}{e_f}\right)\right]\times \left[-\frac{e_g}{e_f}-\frac{h}{e_f\sqrt{i\omega}}+\frac{e_s}{e_f}+e^{2q_sL_s}\left(\frac{e_g}{e_f}+\frac{h}{e_f\sqrt{i\omega}}+\frac{e_s}{e_f}\right)\right] \tag{7g}$$

$$C1=\frac{e_p}{e_f}\cosh\left(q_pL_p\right)\left\{2\frac{e_s}{e_f}\left(\frac{e_g}{e_f}+\frac{h}{e_f\sqrt{i\omega}}\right)\cosh\left(q_sL_s\right)+\left[\left(\frac{e_g}{e_f}+\frac{h}{e_f\sqrt{i\omega}}\right)^2+\left(\frac{e_s}{e_f}\right)^2\right]\sinh\left(q_sL_s\right)\right\} \tag{7h}$$

$$D1=\sinh\left(q_pL_p\right)\left\{\frac{e_s}{e_f}\left[\left(\frac{e_g}{e_f}+\frac{h}{e_f\sqrt{i\omega}}\right)^2+\left(\frac{e_p}{e_f}\right)^2\right]\cosh\left(q_sL_s\right)+\left(\frac{e_g}{e_f}+\frac{h}{e_f\sqrt{i\omega}}\right)\left[\left(\frac{e_p}{e_f}\right)^2+\left(\frac{e_s}{e_f}\right)^2\right]\sinh\left(q_sL_s\right)\right\} \tag{7i}$$

Note that in the normalized signal the frequency dependence of the detection electronics is removed since factors *a* and *b* are simplified. Moreover, the normalized signal does not depend on the laser intensity $I_o$ either. As can be seen, Eqs. (6) and (7) have been written in such a way that the correlation between parameters can be clearly appreciated. Actually, $S_n$ depends on seven parameters: $x_s=L_s/\sqrt{D_s}$, $x_f=L_f/\sqrt{D_f}$, $x_p=L_p/\sqrt{D_p}$, $e_g/e_f$, $e_s/e_f$, $e_p/e_f$ and $h$. Since $L_s$, $L_p$, $D_p$, $e_p$, $e_g$ and $e_f$ are known, only four unknown parameters remain: the fluid "thermal thickness" $x_f$, the heat losses coefficient $h$, the sample effusivity $e_s$ and the sample diffusivity $D_s$. Therefore, a fitting of the frequency behaviour of the normalized PPE signal, $S_n$, to Eq. (6) allows retrieving $e_s$ and $D_s$ together with $x_f$ and $h$ as a by-products.

## 3. Numerical simulations

In the following, all the numerical simulations are performed for a $LiTaO_3$ pyroelectric sensor ($L_p$ = 0.32 mm, $D_p$ = 1.50 mm$^2$/s and $e_p$ = 3750 Ws$^{0.5}$m$^{-2}$K$^{-1}$) and a high-conductive silicone grease ($e_f$ = 980 Ws$^{0.5}$m$^{-2}$K$^{-1}$), which are used in the experimental setup at room temperature. Moreover, in the simulations, we use realistic values of the "thermal thickness" of the fluid ($x_f$ = 0.01 s$^{0.5}$, which means a fluid thickness $L_f \approx 5$ μm, since $D_f \approx 0.2$ mm$^2$/s) and $h$ = 10 Wm$^{-2}$K$^{-1}$. Fig. 2 shows the frequency dependence of the amplitude, $|S_n|$, and phase, $\Psi_n$, of the normalized PPE for solids with effusivities $e_s$ = 2000 and 1000 Ws$^{0.5}$m$^{-2}$K$^{-1}$. For each effusivity, three values of the solid "thermal thickness" are analyzed: $x_s$= 0.3, 0.8 and ∞ s$^{0.5}$. As can be observed, at high frequencies $|S_n|$ = 1 and $\Psi_n$ = 0, since the thermal wave does not emerge from the pyroelectric sensor and therefore the PPE signal is insensitive to the solid sample placed on top of the pyroelectric sensor. At low frequencies, instead, the PPE signal is

highly affected by the thermophysical properties of the solid sample ($e_s$ and $x_s$). As can be seen in Fig. 2, for a solid sample of finite thickness ($x_s < \infty$) $|S_n|$ shows a quasi-sigmoid shape while $\Psi_n$ exhibits a maximum at intermediate frequencies. For a given $e_s$ value, the phase maximum is enhanced and shifted to lower frequencies as $x_s$ increases. However, for a fixed $x_s$ value, the phase maximum is only enhanced (not shifted) as $e_s$ increases.

Fig. 3 analyzes the influence of the fluid "thermal thickness" and the heat losses on the frequency dependence of the PPE signal. These simulations are performed for a solid sample with $e_s$ = 2000 $Ws^{0.5}m^{-2}K^{-1}$ and $x_s$= 0.8 $s^{0.5}$. In Fig. 3a the heat losses coefficient is kept fixed $h$ = 10 $Wm^{-2}K^{-1}$ while fluid "thermal thickness" varies: $x_f$ = 0.01, 0.02 and 0.05 $s^{0.5}$. These values correspond to realistic grease thicknesses going from 5 to 25 μm. As can be observed, its effect on the PPE signal is small but not negligible, so it must be taken into account in the fitting procedure. Similarly, in Fig. 3b the fluid "thermal thickness" is kept fixed $x_f$ = 0.05 $s^{0.5}$ while the coefficient of heat losses varies: $h$ = 0, 10 and 20 $Wm^{-2}K^{-1}$. They correspond to realistic coefficients accounting for radiation and natural convection at room temperature. As can be seen, the influence of heat losses in the amplitude of the PPE signal is negligible whereas in the phase it is concentrated at very low frequencies. Anyway, it will be taken into consideration in the fitting procedure.

As the aim of this work is to measure $e_s$ and $D_s$ from the frequency dependence of the PPE signal and taking into account that, according to Eq. (6), it depends on four free parameters ($e_s$, $x_s$, $x_f$ and $h$) it is mandatory to verify that those parameters are not correlated. To do this, we calculate the reduced sensitivity of the of the amplitude and phase of the PPE signal to a given quantity $x$, which is defined as [13]

$$S^Z(x) = x\frac{\partial Z}{\partial x}, \quad \text{with } Z = |S_n| \text{ or } \Psi_n \text{ and } x = e_s, x_s, x_f \text{ or } h. \tag{8}$$

Fig. 4 shows the numerical simulations of the frequency scan of the sensitivity of the PPE signal to the four free parameters ($x_s$, $e_s$, $x_f$ and $h$). Calculations have been performed with $x_s$ = 0.5 $s^{0.5}$, $e_s$ = 2000 $Ws^{0.5}m^{-2}K^{-1}$, $x_f$ = 0.01 $s^{0.5}$, $h$ = 10 $Wm^{-2}K^{-1}$. The amplitude sensitivity and the phase sensitivity are shown separately in Figs. 4a and 4b respectively. As can be observed, the sensitivities to $x_s$ and $e_s$ are not proportional, indicating that they are not correlated. Moreover, the sensitivities to $x_f$ and $h$ are very small, provided that both quantities remain realistically bounded: $L_f$ < 25 μm and h < 20 $Wm^{-2}K^{-1}$.

Fig. 5 shows the numerical simulations of the frequency scan of the sensitivity of the amplitude and phase of the PPE signal to $x_s$. Calculations have been performed with $e_s$ = 2000 $Ws^{0.5}m^{-2}K^{-1}$, $x_f$ = 0.01 $s^{0.5}$ and $h$ = 10 $Wm^{-2}K^{-1}$. Five values of the sample "thermal thickness" are analyzed: 2, 1, 0.75, 0.5 and 0.25 $s^{0.5}$. As can be observed, both amplitude and phase sensitivities are shifted to lower frequencies as $x_s$ rises. However, while the maximum sensitivity in amplitude remains almost constant, the phase sensitivity increases as $x_s$ rises. Accordingly, it would be expected that using quite thin samples leads to accurate $x_s$, and therefore $D_s$, values. However, working at very low frequencies requires long acquisition times. This drawback together with the presence of the $1/f$ noise and the need of wide sensor and sample to keep the 1D model makes it advisable to work with $x_s$ values in the range 0.4 - 0.8 $s^{0.5}$.

Fig. 6 shows the numerical simulations of the frequency scan of the sensitivity of the amplitude and phase of the PPE signal to $e_s$. Calculations have been performed with $x_s$ = 0.5 $s^{0.5}$, $x_f$ = 0.01 $s^{0.5}$ and $h$ = 10 $Wm^{-2}K^{-1}$. Five values of the sample effusivity are analyzed: 10000, 5000, 2000, 1000, 500 $Ws^{0.5}m^{-2}K^{-1}$. Regarding the amplitude, the highest sensitivity to $e_s$ arises for samples with a similar effusivity as the pyroelectric sensor. This sensitivity decreases as the sample effusivity differs from the pyroelectric sensor's effusivity. The phase sensitivity, instead, monotonously increases with the sample effusivity and the maximum sensitivity is shifted to lower frequencies.

## 4. Experimental results and discussion

In order to verify the validity of the method we have performed PPE measurements on a set of samples, covering a wide range of thermal properties: poly-ether-ether-ketone (PEEK), BK7 glass, $LiTaO_3$ single crystal and glassy carbon. Besides, to check the robustness of the method, for each material, we have performed measurements on samples with varying thicknesses. The samples are placed on top of a $LiTaO_3$ pyroelectric crystal plate with dimensions 1.6×1.6×0.32 $mm^3$. A very thin layer of high-conductive silicone grease (Heat sink compound, Dow Corning) is used to assure the thermal contact. A diode laser ($\lambda$ = 656 nm, 50 mW) is directed to the free pyroelectric surface, heating a circular area of about 7 mm in diameter. Its intensity is modulated by a periodic current governed by the computer and serving as the lock-in reference. The PPE current produced by the detector has been fed into a digital lock-in amplifier.

Both, the amplitude, $|S_n|$, and the phase, $\Psi_n$, of the normalized signal are fitted simultaneously to retrieve the thermal effusivity and diffusivity. All measurements have been performed at room temperature. In order to avoid lateral boundary effects, the lowest frequency we used was 0.4 Hz. Logarithmic spacing of data points on frequency scans has been used since it has been demonstrated to be superior to linear spacing [14]. Due to the high sensitivity and low noise of the $LiTaO_3$ sensor together with the noise reduction provided by the lock-in amplifier, the data amplitude noise remains lower than 1‰ and the phase noise smaller than 0.05º.

Fig. 7 shows the room temperature frequency scans of the amplitude and phase of the normalized PPE signal for BK7 glass samples with varying thicknesses. Dots are the experimental data and the continuous lines are the fits to Eq. (6). The retrieved values of the thermal properties are given in table 1, and correspond to the average values from five frequency scans after changing the coupling grease each time. They are consistent and in good agreement with the tabulated values [15]. Note that the signal phase is much more sensitive to the thermal properties than the signal amplitude, in agreement with the sensitivity analysis performed in the previous section. On the other hand, the thermal effusivity is obtained with high precision regardless the thickness of the sample. The precision in the thermal diffusivity, instead, depends on the sample thickness. For the 2.85 mm thick sample no information on the thermal diffusivity is obtained, since the sample is thermally thick in the whole frequency range (the phase maximum is absent). As the thickness is reduced, the maximum in the signal phase appears clearly. However, for the 0.677 mm thick sample, the maximum in phase is located just at the lower frequency limit and therefore the thermal diffusivity is slightly overestimated. For the other three thicknesses (0.466, 0.293 and 0.249 mm) the phase maximum is completely developed and the thermal diffusivity is obtained accurately. From these results one can conclude that accurate thermal diffusivity values require the thickness of the sample to be selected in such a way that the phase maximum is located above 1 Hz. Finally, it is worth mentioning that in all measurements $x_f$ falls in the range 0.01-0.02 $s^{0.5}$, which corresponds to reasonable grease thicknesses of 5-10 μm, and $h$ in the range 5-15 $Wm^{-2}K^{-1}$.

In Fig. 8 we show the frequency scans of the amplitude and phase of the normalized PPE signal for the rest of the solids studied in this work. Dots are the experimental data and the continuous lines are the fits to Eq. (6). The retrieved values of the thermal properties are given in table 1. As can be seen, they are consistent and in good agreement with the literature values [16,17]. Note that for the sake of clarity not all the samples included in table 1 are shown in Fig. 8.

It is worth emphasising that this method based on a frequency scan of the PPE signal in the front configuration is valid for all kind of solids regardless their thermal properties.

However, in this work we have not shown results on high thermal conductors (metals, alloys, ceramics, etc.) because of the limited size of the pyroelectric sensor, which is unable to guarantee 1D heat propagation at low frequencies. Actually, we performed frequency scans for Ni and graphite, but the shape of the phase at low frequencies (0.4 - 1 Hz) could not be fitted to Eq. (6), indicating the presence of border effects. Accordingly, measuring good thermal conductors requires using a larger pyroelectric sensor.

There are two main sources for the uncertainty of the effusivity values in Table 1. One comes from the uncertainty of the known parameters ($L_p$, $D_p$, $e_p$ and $e_f$) and the other one from the standard deviation corresponding to performing several frequency scans. In the fitting procedure we have used as known parameters $L_p$ = 0.32±0.01 mm, $D_p$ = $1.50\times10^{-6}\pm0.10\times10^{-6}$ $m^2/s$, $e_p$ = 3750±100 $Ws^{0.5}m^{-2}K^{-1}$ and $e_f$ = 980±8 $Ws^{0.5}m^{-2}K^{-1}$. To retrieve the thermal diffusivity and effusivity of solids we have used the mean value of each known quantity. However, we have checked the influence of using the extreme values of each parameter, e.g. $L_p$ = 0.33 mm, $D_p$ = $1.6\times10^{-6}$ $m^2/s$, $e_p$ = 3850 $Ws^{0.5}m^{-2}K^{-1}$ and $e_f$ = 972 $Ws^{0.5}m^{-2}K^{-1}$. For most extreme combinations the fits are not good, i.e. the residuals of the fitting are too high. This fact restricts the practical values of the four known parameters. From the trials performed on each sample we can conclude that the uncertainty in $e_s$ coming from the uncertainty in the known parameters is around 2%. On the other hand, for each sample we have performed five frequency scans after changing the coupling grease each time. The standard deviation varies from about 3% for thermal effusivity to about 6% in thermal diffusivity. By adding both uncertainties, we obtain 5% for thermal effusivity to about 8% in thermal diffusivity.

In this work we have demonstrated that the front configuration is useful to measure $D$ and $e$ in solids. However, it raises the question of which method is more appropriate to measure $D$ and $e$ in solids from one frequency scan: the front or the back configuration. The main advantage of the back configuration is its simplicity. Both the natural logarithm of the amplitude, $\mathrm{Ln}|S_n|$, and the phase $\Psi_n$, of the normalized signal behave linearly as a function of $\sqrt{f}$. The common slope gives the thermal diffusivity whereas the vertical offset between both parallel straight lines gives the thermal effusivity [2,18]. A multiparametric fitting to a model is not needed. A second benefit of the back configuration is that, for a given frequency, the signal phase only depends on the thermal diffusivity of the solid. This means that measuring the evolution of the thermal diffusivity with temperature only requires recording the signal phase while the solid temperature varies. Phase variations are directly related to thermal diffusivity changes [2]. Accordingly, the back configuration is well suited to study phase transitions [19]. Anyway, the back configuration suffers from several limitations when dealing with solid samples. First of all, the coupling grease layer reduces the phase slope leading to an underestimation of the thermal diffusivity [5]. Second, as the pyroelectric sensor and the sample have different reflection coefficients, the normalized signal depends on the reflection coefficient ratio and therefore the vertical shift between $\mathrm{Ln}|S_n|$ and $\Psi_n$ gives an inaccurate value of the thermal effusivity. Third, as the linear behaviour arises when the sample is thermally thick, the signal is weak and is affected by parasitic signals (stray laser light, piezoelectric contribution, electromagnetic pick-up, etc.). On the contrary, although the front configuration requires a multiparametric fitting to the model, it produces a high signal insensitive to parasitic contributions. Besides, as the laser only heats the pyroelectric sensor, there are no problems associated to the reflection coefficient ratio. Moreover, as the effect of the grease is included in the model, $D$ and $e$ are obtained with high accuracy.

## 5. Conclusions

This work is focused on the simultaneous measurement of the thermal diffusivity and effusivity of solids using the PPE technique in the front configuration. A complete theoretical

model of the PPE signal generation has been developed. It takes into account the effect of the thin fluid layer used to thermally couple the pyroelectric sensor and the test solid, the effect of heat conduction to the surrounding air and the effect of heat losses by convection and radiation. To verify the validity of the method, we have measured the thermal diffusivity and effusivity of a set of solids covering a wide range of thermal properties. The method is robust since the same thermal properties are obtained when varying the thickness of the sample and it is also accurate because the retrieved values are in good agreement with the literature values.

## Acknowledgments

This work has been supported by Ministerio de Economía y Competitividad, (DPI2016-77719-R, AEI/FEDER, UE), by Gobierno Vasco (KK-2016/00027) and by Universidad del País Vasco UPV/EHU (GIU16/33).

## References


[1] A. Mandelis and M.M. Zver, Theory pf photopyroelectric spectroscopy of solids, J. Appl. Phys. **57**, 4421-4430 (1985).
[2] M. Marinelli, F. Murtas, M.G. Mecozzi, U. Zammit, R. Pizzoferrato and F. Scudieri, Simultaneous determination of specific heat, thermal conductivity and thermal diffusivity at low temperature via the photopyroelectric technique, Appl. Phys. A **51**, 387-393 (1990).
[3] S. Delenclos, M. Chirtoc, A. Hadj Sahraoui, C. Kolinski and J.M. Buisine, A new calibration procedure for the determination of thermal parameters and their temperature dependence using the photopyroelectric method, Anal. Sci. **17**, s161-s164 (2001).
[4] U. Zammit, M. Marinelli, F. Mercuri, S. Paoloni and F. Scudieri, Invited Review Article: Photopyroelectric calorimetry for the simultaneous thermal, optical and structural characterization of samples over phase transitions, Rev. Sci. Instrum. **82**, 121101 (2011).
[5] A. Salazar, On the influence of the coupling fluid in photopyroelectric measurements, Rev. Sci. Instrum. **74**, 825-827 (2003).
[6] A. Salazar and A. Oleaga, Overcoming the influence of the coupling fluid in photopyroelectric measurements of solid samples, Rev. Sci. Instrum. **83**, 014903 (2012).
[7] D. Dadarlat, M. Chirtoc, C. Nematu, R.M. Candea and D. Bicanic, Inverse photopyroelectric detection method, Phys. Status Solidi A, **121**, K231-235 (1990).
[8] A. Hadj Sahraoui, S. Longuemart, D. Dadarlat, S. Delenclos, C. Kolinsky and J.M. Buisine, The application of the photopyroelectric method for measuring the thermal parameters of pyroelectric materials, Rev. Sci. Instrum. **73**, 2766-2772 (2002).
[9] D. Dadarlat and C. Neamtu, Detection of molecular associations in liquids by photopyroelectric measurements of thermal effusivity, Meas. Sci. Technol. **17**, 3250-3254 (2006).
[10] D. Dadarlat, C. Neamtu, M. Streza, R. Turcu, I. Craciunescu, D. Bica and L. Vekas, High accuracy photopyroelectric investigation of dynamic termal parameters of FeO and CoFeO magnetic nanofluids, J. Nanopart. Res. **10**, 1329-1336 (2008).
[11] A. Salazar, A. Oleaga, V. Shvalya and E. Apiñaniz, Improved thermal effusivity measurements of solids using the photopyroelectric technique in the front configuration, Int. J. Therm. Sci. **100**, 60-65 (2016).
[12] M. Chirtoc and G. Mihailescu, Theory of the photopyroelectric method for investigation of optical and thermal materials properties, Phys. Rev. B **40**, 9606-9617 (1989).
[13] M. N. Özisik and H.R.B. Orlande, Inverse Heat Transfer, Taylor & Francis, New York (2000), p. 53.
[14] K. Horne, A. Fleming, B. Timmins and H. Ban, Monte Carlo uncertainty analysis for photothermal radiometry measurements using curve fit process, Metrologia **52**, 783-792 (2015).
[15] F. Hemberger, A. Göbel and H.P. Ebert, Determination of the thermal diffusivity of electrically non-conductive solids in the temperature range from 80 K to 300 K by laser-flash measurement, Int. J. Thermophys. **31**, 2187-2200 (2010).
[16] N.W. Pech-May, A. Cifuentes, A. Mendioroz, A. Oleaga and A. Salazar, Simultaneous measurement of thermal diffusivity and effusivity of solids using the flash technique in the front-face configuration, Meas. Sci. Technol. **26**, 085017 (2015).
[17] Goodfellow catalogue www.goodfellow.com
[18] S. Delenclos, M. Chirtoc, A. Hadj Sahraoui, C. Kolinski and J.M. Buisine, Assessment of calibration procedures for accurate determination of thermal parameters of liquids and their temperature dependence using the photopyroelectric method, Rev. Sci. Instrum. **73**, 2773-2780 (2002).

[19] U. Zammit, M. Marinelli, F. Mercuri, S. Paoloni and F. Scudieri, Invited Review Article: Photopyroelectric calorimetry for the simultaneous thermal, optical and structural characterization of samples over phase transitions, Rev. Sci. Instrum. **82**, 121101 (2011).

## Figure Captions

Fig. 1. Geometry of the photopyroelectric cell in the front configuration.

Fig. 2. Numerical simulations of the frequency dependence of the amplitude, $|S_n|$, and phase, $\Psi_n$, of the normalized PPE signal. Three values of the solid "thermal thickness" $x_s$ are considered. For each thermal thickness two effusivity values are simulated: $e_s$ = 2000 $Ws^{0.5}m^{-2}K^{-1}$ (continuous lines) and $e_s$ = 1000 $Ws^{0.5}m^{-2}K^{-1}$ (dotted lines).

Fig. 3. Numerical simulations of the frequency dependence of the amplitude, $|S_n|$, and phase, $\Psi_n$, of the normalized PPE signal showing the influence of the coupling fluid thickness (a) and heat losses (b). Simulations are performed for $e_s$ = 2000 $Ws^{0.5}m^{-2}K^{-1}$ and $x_s$= 0.8 $s^{0.5}$. (a) Heat losses are kept fixed $h$ = 10 $Wm^{-2}$ $K^{-1}$ while $x_f$ varies. (b) $x_f$ is kept fixed $x_f$ = 0.01 $s^{0.5}$ while $h$ varies.

Fig. 4. Numerical simulations of the frequency dependence of the sensitivity of the PPE signal to the four free parameters ($x_s$, $e_s$, $x_f$ and $h$). Calculations have been performed with $x_s$ = 0.5 $s^{0.5}$, $e_s$ = 2000 $Ws^{0.5}m^{-2}K^{-1}$, $x_f$ = 0.01 $s^{0.5}$, $h$ = 10 $Wm^{-2}$ $K^{-1}$. (a) Amplitude sensitivity and (b) phase sensitivity.

Fig. 5. Numerical simulations of the frequency dependence of the sensitivity of the amplitude and phase of the PPE signal to $x_s$. Calculations have been performed with $e_s$ = 2000 $Ws^{0.5}m^{-2}K^{-1}$, $x_f$ = 0.01 $s^{0.5}$ and $h$ = 10 $Wm^{-2}$ $K^{-1}$. Five values of the sample "thermal thickness" are analyzed.

Fig. 6. Numerical simulations of the frequency dependence of the sensitivity of the amplitude and phase of the PPE signal to $e_s$. Calculations have been performed with $x_s$ = 0.5 $s^{0.5}$, $x_f$ = 0.01 $s^{0.5}$ and $h$ = 10 $Wm^{-2}$ $K^{-1}$. Five values of the sample effusivity are analyzed.

Fig. 7. Experimental frequency scans of the amplitude and phase of the normalized PPE signal for the same BK7 glass with five different thicknesses. Dots are the experimental data and solid lines are the fits to Eq. (6).

Fig. 8. The same as in Fig. 7 for two samples of $LiTaO_3$ single crystal and two samples of PEEK. Dots are the experimental data and solid lines are the fits to Eq. (6).

Table 1. Room temperature thermal diffusivity ($D_s$) and effusivity ($e_s$) of the materials studied in this work. The uncertainty is 5% for $e_s$ and 8% for $D_s$.

| Material | $L_s$ (mm) | $D_s$ ($mm^2s^{-1}$) | $D_s$ Literature[a] ($mm^2s^{-1}$) | $e_s$ ($Ws^{0.5}m^{-2}K^{-1}$) | $e_s$ Literature[a] ($Ws^{0.5}m^{-2}K^{-1}$) |
|---|---|---|---|---|---|
| BK7 glass | 2.85 | - | 0.54 | 1300 | 1375 |
| BK7 glass | 0.677 | 0.59 | 0.54 | 1320 | 1375 |
| BK7 glass | 0.466 | 0.56 | 0.54 | 1310 | 1375 |
| BK7 glass | 0.293 | 0.55 | 0.54 | 1330 | 1375 |
| BK7 glass | 0.249 | 0.55 | 0.54 | 1300 | 1375 |
| | | | | | |
| $LiTaO_3$ | 0.508 | 1.48 | 1.50 | 3750 | 3750 |
| $LiTaO_3$ | 0.413 | 1.51 | 1.50 | 3720 | 3750 |
| $LiTaO_3$ | 0.302 | 1.50 | 1.50 | 3800 | 3750 |
| | | | | | |
| PEEK | 0.480 | - | 0.18 | 600 | 640 |
| PEEK | 0.255 | 0.18 | 0.18 | 605 | 640 |
| PEEK | 0.127 | 0.17 | 0.18 | 610 | 640 |
| | | | | | |
| Sigradur G | 5.980 | - | 6.3 | 2560 | 2530 |
| Sigradur G | 1.300 | 6.2 | 6.3 | 2550 | 2530 |
| Sigradur G | 0.827 | 6.0 | 6.3 | 2570 | 2530 |
| | | | | | |

[a]References [15-17]

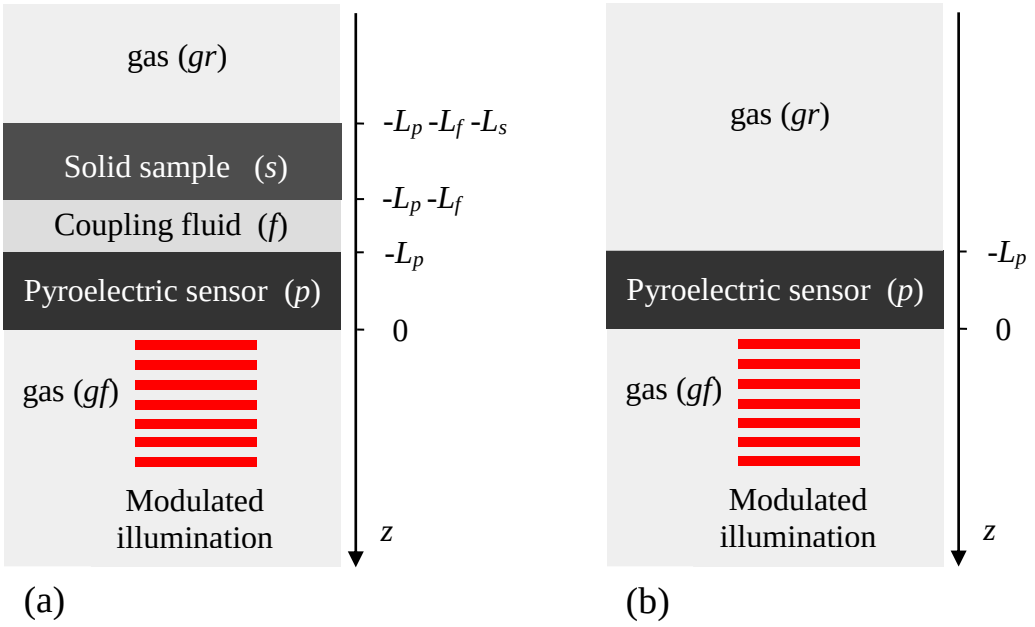
gas (gr)
Solid sample (s)
Coupling fluid (f)
Pyroelectric sensor (p)
gas (gf)
Modulated illumination
-Lp -Lf -Ls
-Lp -Lf
-Lp
0
z
(a)
gas (gr)
Pyroelectric sensor (p)
gas (gf)
Modulated illumination
-Lp
0
z
(b)

Fig. 1

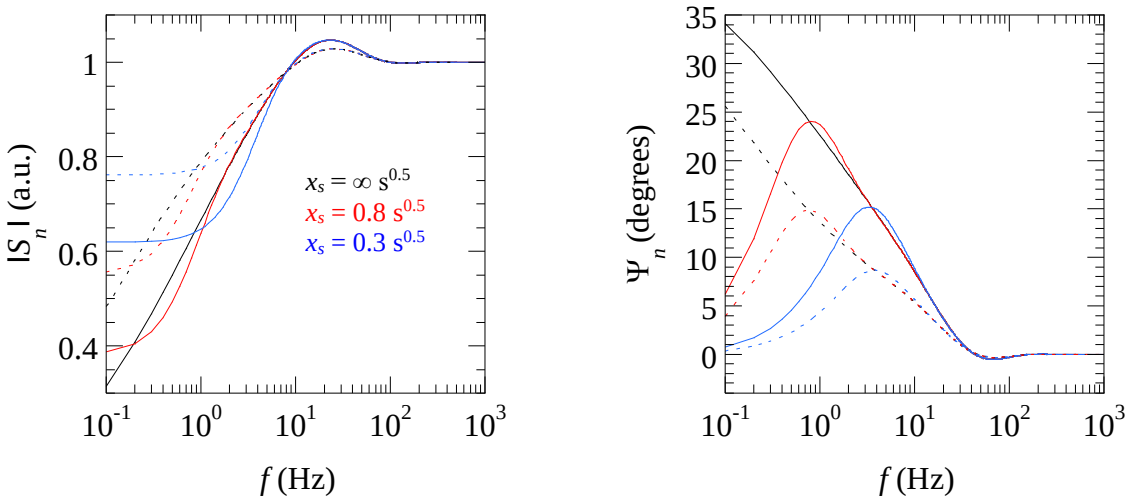
|S|n (a.u.)
1
0.8
0.6
0.4
xs = ∞ s0.5
xs = 0.8 s0.5
xs = 0.3 s0.5
10-1
100
101
102
103
f (Hz)
Ψn (degrees)
35
30
25
20
15
10
5
0
10-1
100
101
102
103
f (Hz)

Fig. 2

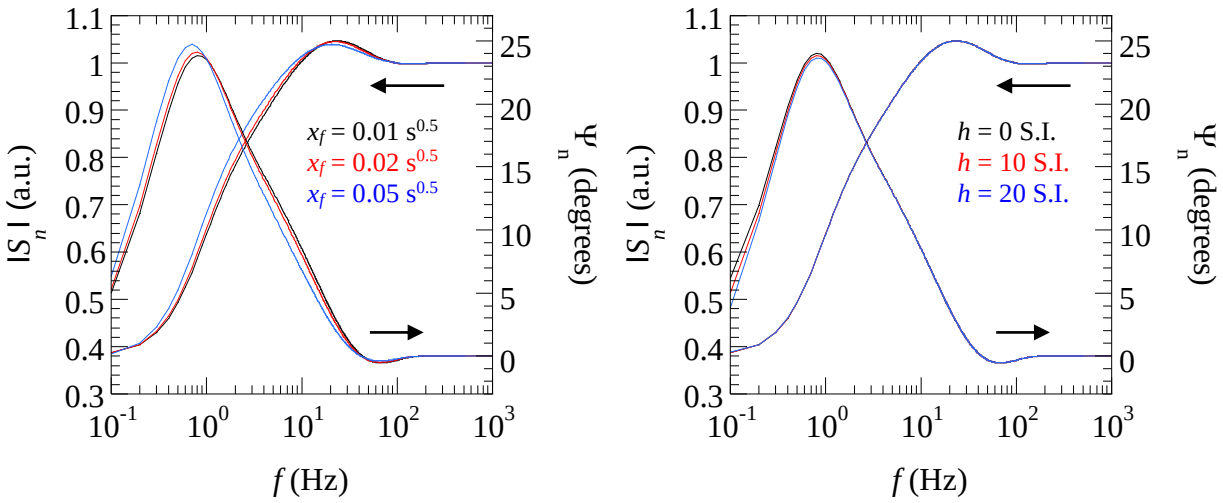


(a) (b)

Fig. 3

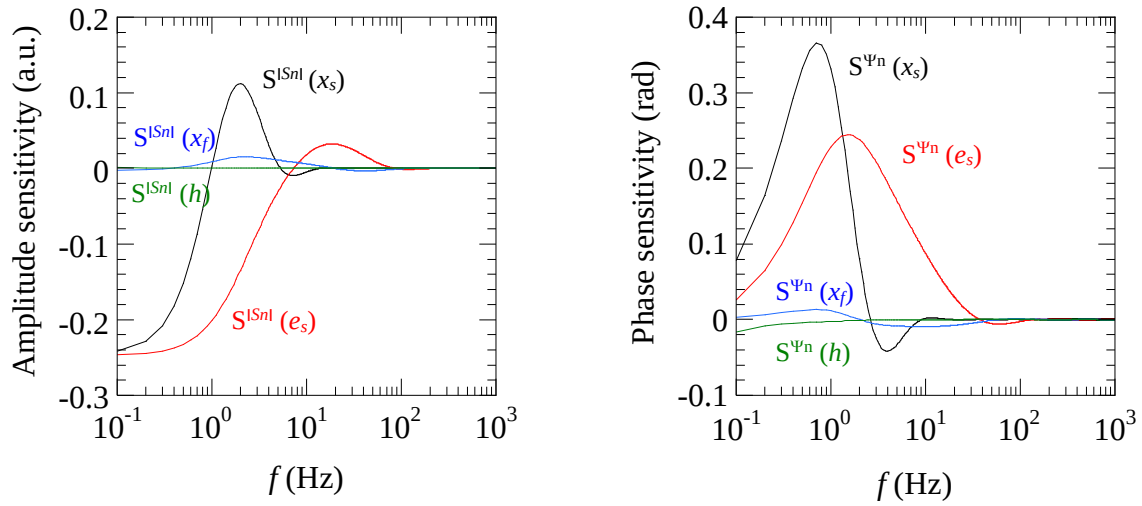


(a) (b)

Fig. 4

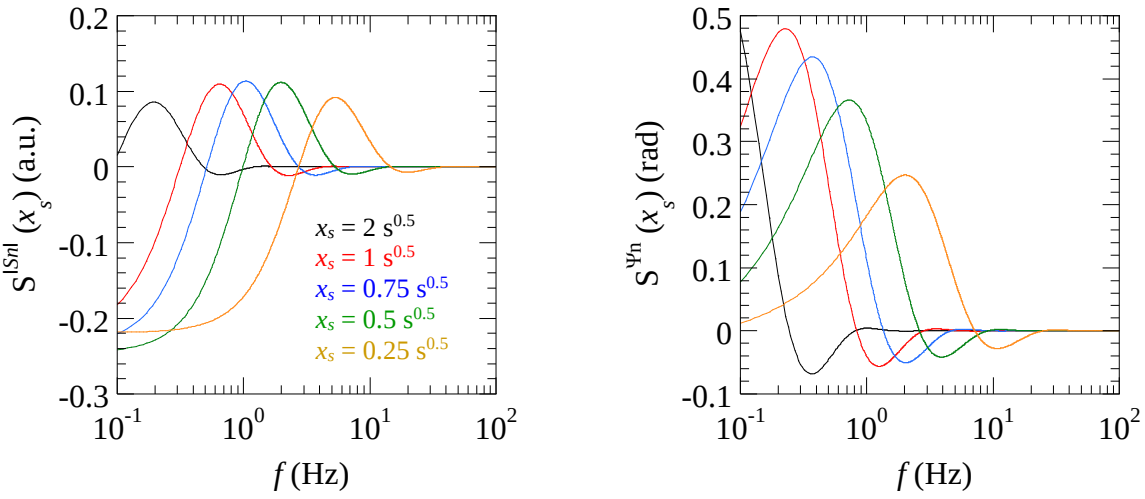
0.2
0.1
0
-0.1
-0.2
-0.3
$10^{-1}$
$10^{0}$
$10^{1}$
$10^{2}$
$f$ (Hz)
$S^{|Sn|}(x_s)$ (a.u.)
$x_s$ = 2 $s^{0.5}$
$x_s$ = 1 $s^{0.5}$
$x_s$ = 0.75 $s^{0.5}$
$x_s$ = 0.5 $s^{0.5}$
$x_s$ = 0.25 $s^{0.5}$
0.5
0.4
0.3
0.2
0.1
0
-0.1
$S^{\Psi n}(x_s)$ (rad)

Fig. 5

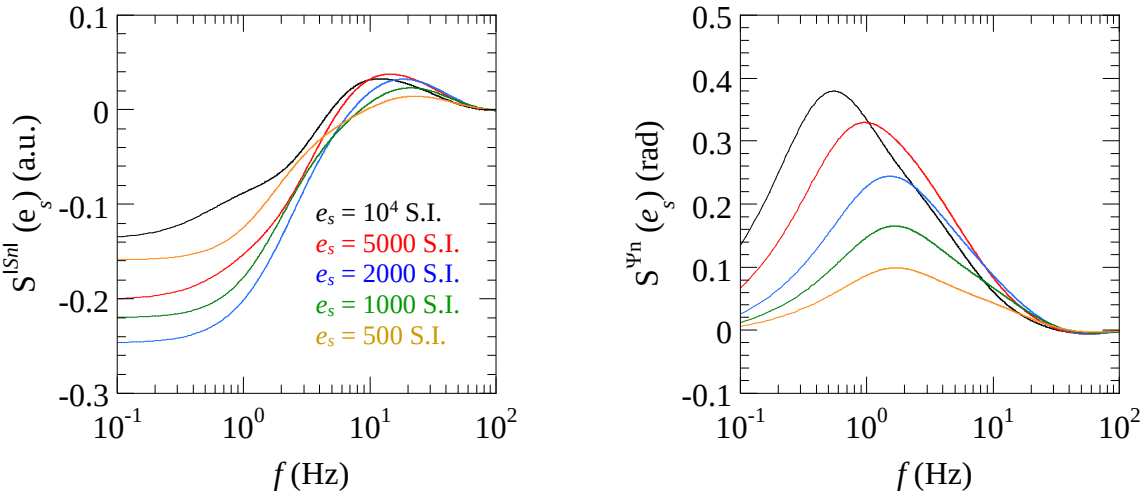
0.1
0
-0.1
-0.2
-0.3
$10^{-1}$
$10^{0}$
$10^{1}$
$10^{2}$
$f$ (Hz)
$S^{|Sn|}(e_s)$ (a.u.)
$e_s$ = $10^4$ S.I.
$e_s$ = 5000 S.I.
$e_s$ = 2000 S.I.
$e_s$ = 1000 S.I.
$e_s$ = 500 S.I.
0.5
0.4
0.3
0.2
0.1
0
-0.1
$S^{\Psi n}(e_s)$ (rad)

Fig. 6

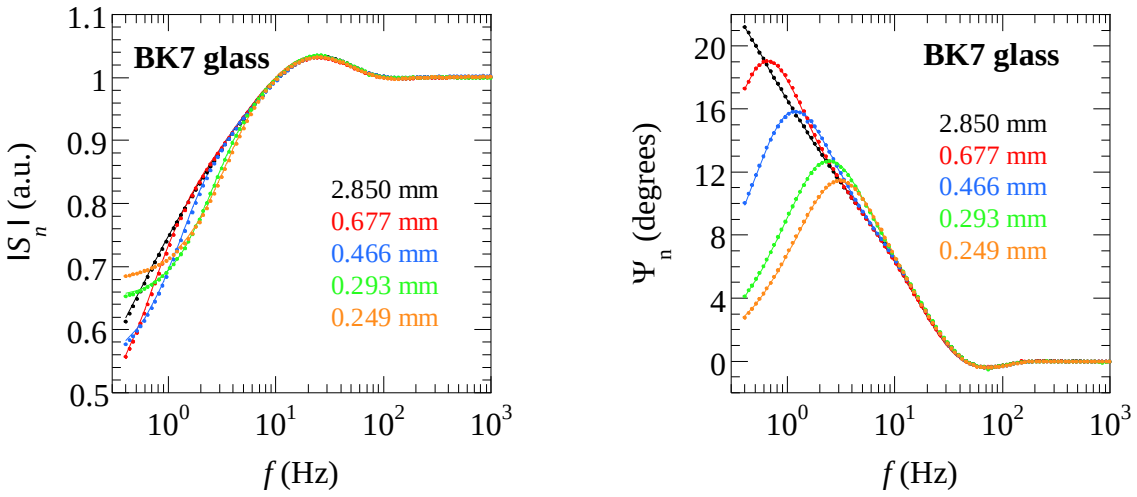
BK7 glass
2.850 mm
0.677 mm
0.466 mm
0.293 mm
0.249 mm
|S|n (a.u.)
Ψn (degrees)
f (Hz)

Fig. 7

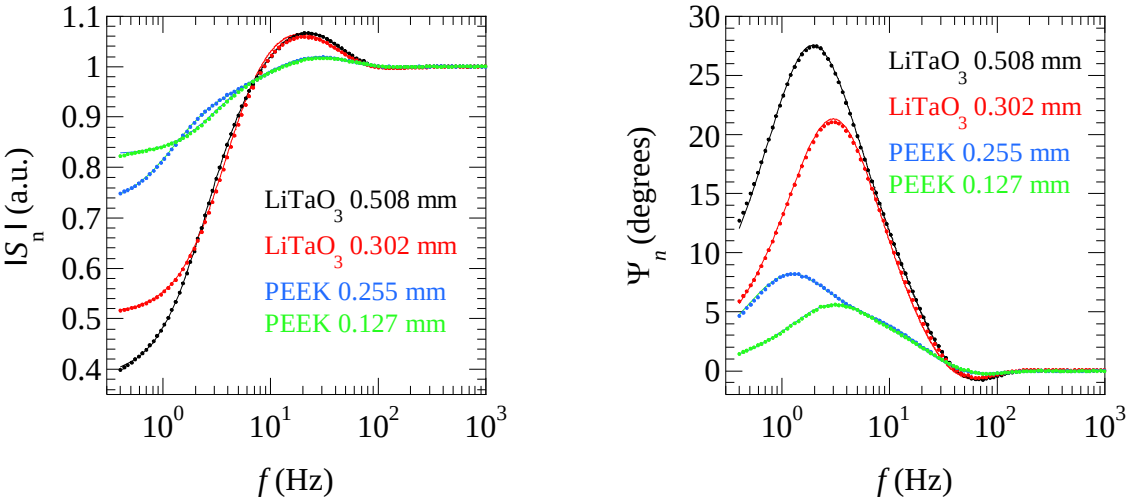
LiTaO3 0.508 mm
LiTaO3 0.302 mm
PEEK 0.255 mm
PEEK 0.127 mm
|S|n (a.u.)
Ψn (degrees)
f (Hz)

Fig. 8